Artificially smart optimization of crash cushion device sustained by experimental and numerical study of re-entrant auxetic honeycomb

Jeanne Tondut, Noëlie Di Cesare, Sylvie Ronel

TCRS#2134690, VOL 0, ISS 0

Artificially smart optimization of crash cushion device sustained by experimental and numerical study of re-entrant auxetic honeycomb

J. Tondut, N. Di Cesare, and S. Ronel

QUERY SHEET

This page lists questions we have about your paper. The numbers displayed at left are hyperlinked to the location of the query in your paper.

The title and author names are listed on this sheet as they will be published, both on your paper and on the Table of Contents. Please review and ensure the information is correct and advise us if any changes need to be made. In addition, please review your paper as a whole for typographical and essential corrections.

Your PDF proof has been enabled so that you can comment on the proof directly using Adobe Acrobat. For further information on marking corrections using Acrobat, please visit https://authorservices.taylorandfrancis.com/how-to-correct-proofs-with-adobe/

The CrossRef database (www.crossref.org/) has been used to validate the references.

AUTHOR QUERIES

Q1 Please check and confirm whether the author affiliations and corresponding details have been set correctly.

Q2 The disclosure statement has been inserted. Please correct if this is inaccurate.

Q3 Please provide missing editor names, publisher name and location for the "Parsopoulos and Vrahatis 2002" references list entry.

Q4 Figures 4, 3, 20, 21, and 19 have been changed to Figures 3, 4, 19–21 to maintain sequential. Please check.

INTERNATIONAL JOURNAL OF CRASHWORTHINESS
https://doi.org/10.1080/13588265.2022.2134690

Artificially smart optimization of crash cushion device sustained by experimental and numerical study of re-entrant auxetic honeycomb

J. Tondut[a], N. Di Cesare[b] and S. Ronel[a]

[a]LBMC UMR_T 9406, Université Claude Bernard Lyon 1, Univ. Eiffel, Lyon, France; [b]LMC2 EA 7427, Université Claude Bernard Lyon 1, Lyon, France

ABSTRACT

Honeycomb structures are widely used in energy absorption, and more recently auxetic honeycombs have been studied in order to improve absorption capabilities of such structures. The hexagonal re-entrant (HR) honeycomb is foreseen to be a promising structure under impact velocities. An experimental analysis of the re-entrant honeycomb under impact velocity has led to a finite elements model validation at scale one, i.e. scale of current car crash cushions. A new objective function based on the European Standard has been developed in order to improve crash cushions capabilities while avoiding peak deceleration by using a meta-heuristic optimization algorithm. The global optimization process has been performed using Inverse-PageRank-PSO algorithm. The algorithm has led to an optimal geometrical configuration of HR honeycomb improving the performance of current road safety devices. The optimal structure presents a quasi-linear absorption curve, as recommended by European standards.

ARTICLE HISTORY
Received 17 February 2022
Accepted 24 September 2022

KEYWORDS
Optimization; energy absorption; hexagonal re-entrant honeycomb; road safety

1. Introduction

Honeycomb structures are widely used, solicited in-plane, in energy absorption [1–4] and constitute crash cushion systems used along roads. The aim of these devices is to efficiently absorb kinetic energy, while preserving the vehicle occupants integrity. European and French standards [5,6] give the impact conditions and the absorption capabilities of the structure to be validated and installed along roads. To do so, optimization methodologies can be used, to develop the most adapted structure, while considering the manufacturing capabilities of the road safety devices industry. Usually, simple folded metal sheets are assembled [7]. In this paper, a parametric optimization algorithm is used, to find the best geometric parameters of the structure, to improve the structural absorption capabilities, while meeting the European standards and guaranteeing manufacturing constraints.

Cellular materials, such as honeycombs, have been used as new engineered materials because of their very efficient energy absorption capabilities [3,8–10]. In the last few years, many works have been conducted on auxetic materials [11–13], which exhibit a negative Poisson's ratio, since they have been introduced by Lakes et al. [14]. Usually manufactured as foams [15,16], they can also be manufactured at bigger scales, and are then called cellular materials [17]. However, if honeycomb structures can not be considered as a Representative Volume Element, because the scale ratio conditions [18] are not met, the structure has to be entirely considered and no homogenization method is needed [19]. In this paper, the total structure will be studied and optimized. Numerous shapes of auxetic microstructures have been proposed in the literature, such as star honeycomb, arrow-head honeycomb, chiral honeycomb and hexagonal re-entrant honeycomb [13]. Optimization methodologies are sometimes used to design new microstructures exhibiting high negative Poisson's ratio effects [20,21].

The hexagonal re-entrant (HR) honeycomb has shown high efficient capabilities in energy absorption under impact compared to conventional honeycomb [8,10,19,22]. Under quasi-static conditions, many studies have been conducted to predict either the elastic constants [23], or the dependence of hexagonal re-entrant honeycombs' Poisson's ratio and Young's modulus on the cell geometric parameters, using Finite Elements Method (FEM) analysis [17,22]. A theoretical approach to predict negative Poisson's ratios of auxetic honeycombs has been developed, which is based on the large deflection model [2]. Experimental and numerical studies have been performed on the hexagonal re-entrant honeycomb under quasi-static loading to study its crushing behavior. They have investigated the negative Poisson ratio effects on the crushing stress and energy absorption efficiency [19]. If the elastic and quasi-static behaviors of hexagonal re-entrant honeycombs have been largely studied, the dynamic behavior under impact velocities is less studied. Hou et al. [8] and Hu et al. [9] have worked on the dynamic response of re-entrant honeycombs under high velocity crush [8,9]. In these works, the energy absorption efficiency of the structure is computed by using the propagation waves theory. The studied velocities are over

CONTACT S. Ronel sylvie.ronel@univ-lyon1.fr

100 m/s and thus, do not correspond to car limitation speeds which are limited to 30 m/s on highways in France [5]. In fact, European standards impose a certain structural volume and geometry adapted to the impact velocity, which will then be studied in this paper.

In the literature, some studies have been conducted on the optimization of HR honeycomb structures subjected to crash. Wang et al. [24] have optimized a crash-box with 3 D re-entrant auxetic core under 15 and 40 km/h crash conditions. However, the studied volume is limited to the imposed crash-box size, i.e. $(130 \times 133 \times 73mm)$ and does not correspond to crash cushion device volumes $(1200 \times 800 \times 700mm$ under 50 $km/h)$ usually used by car cushion manufacturers [7]. On another hand, Qi et al. [25] have achieved a multi-scale optimization of the hexagonal re-entrant honeycomb under blast impact. In order to improve honeycomb capabilities, a multi-objective function have been designed, to investigate the optimal thickness value of a cell-wall material as an independent variable of the problem. The obtained HR honeycomb structure exhibits an improvement about 5% of the energy absorption compared to conventional honeycomb.

Most of the road networks are lined with many advanced road safety systems. These devices absorb the kinetic energy of crashing cars mostly by plastic deformation. The volume of these safety systems varies as a function of the limitation speed. Currently, these types of cushions are made of conventional honeycomb structures, which absorb kinetic energy essentially by in-plane plastic deformation [7,26]. In this paper, the hexagonal re-entrant honeycomb deformation under car crash impact velocities is investigated to improve the performance of current cushions. The major criterion in car cushion design is about the deceleration felt by the crashed-car-user and is called the Acceleration Sensitivity Index (*ASI*) [5]. The European standard estimates at $9.8 \times g$ $[m/s^{-2}]$ the deceleration that can be sustained during 50 ms by a human being before severe injuries [5], where g is the gravity acceleration. Indeed, in crashworthiness optimization, many works have investigated the Specific Energy Absorption (*SEA*) based on the stress-strain curve optimization [25,27–29]. *SEA* optimization consists of maximizing the integral of the impact force, over the displacement under quasi-static loading while minimizing the mass of the structure. Here, according to the *ASI* criterion, the striker limit force is defined, allowing to characterize the capability of a cushion to absorb kinetic energy. In this paper, this criterion is used to define a new appropriate objective function based on the force-time curve, to be optimized.

The remaining part of this paper is organized as follows. Section 2 presents the experimental study conducted on the HR honeycomb under impact conditions. The experimental work allows to validate the FE model presented in Section 3. The new objective function is defined in Section 4.1, which depends on the design variables defined in Section 4.2. Then, an optimization methodology is performed and presented in Section 5. Finally, the discussion and conclusion of this paper are outlined in Section 6.

2. Experimental analysis of the hexagonal re-entrant honeycomb absorbing cushion device

2.1. Experimental setup

In order to study the mechanical behavior of HR honeycombs under impact conditions, an experimental campaign has been conducted at the LBMC-crash-track [30]. The device is composed of a track propelling a vehicle into a car-cushion-specimen fixed on a concrete wall, as shown in Figure 1. The tested vehicle is a 4-wheel-rigid vehicle with a mass m of 690 kg. The vehicle is freed from the propeller 7 m before the concrete wall, and thus is guided neither during nor after the impact. The 4-wheel-rigid vehicle is propelled at $14m/s$ corresponding to the speed limitation of $50km/h$ defined in the European standards [5,6].

The tested vehicle is instrumented with front and rear accelerometers recording the acceleration of the vehicle in X, Y and Z directions, defined in Figure 1. Acceleration signals are filtered with a Butterworth filter with 4 poles at 180 Hz (BW 4p 180 Hz) in conformity with European standard ISO6487 [31]. The front sensor is able to measure an acceleration up to 500 g whereas the rear sensor has a capacity of 100 g, where g is the gravity acceleration. The sampling interval is $10^{-5}s^{-1}$ for all the accelerometers.

Three high speed video cameras are installed to film different shots. Their corresponding resolutions are described in Table 1. The sampling interval is set to 3000 *images/sec* for all cameras. Cameras are connected to the trigger identifying the beginning of the contact between the vehicle and the specimen. This allows to record 500 images on the cameras before the contact.

Three test patterns are installed on the vehicle in order to automatically track the displacement. The Tracker 5.1.3 software is used with the automated object tracking position functionality to fit the displacements of the test patterns.

2.2. Geometric configuration and manufacturing process of the absorbing cushion device

The unit cell configuration adopted in this study is a re-entrant honeycomb which can be described with three geometric parameters l, h and θ as shown in Figure 2. The cell wall thickness is set to t. By duplicating the unit cell in both X and Y directions, the complete structure is constituted of n and m cells in the X and Y directions respectively. The total lengths of the structure are called L_X, L_Y and L_Z in the X, Y and Z directions respectively.

The specimen dimensions are selected among a set of parameters leading to an absorbing crash-cushion design preserving the experimental devices during impact tests, and are described in Table 2.

The constitutive material used to manufacture the specimen is a certificated (EN 485-2) aluminum (SHEET EN AW 5754 H111) exhibiting a linear elastic isotrope behavior. The Young modulus E, the offset yield point $R_{p0.2}$, the failure stress R_m and the maximal elongation $A\%$ are given in Table 3. The specimen is composed of two major parts. The first one is called wavy sheet and is L_X long and L_Z high.

COLOR Online / B&W in Print

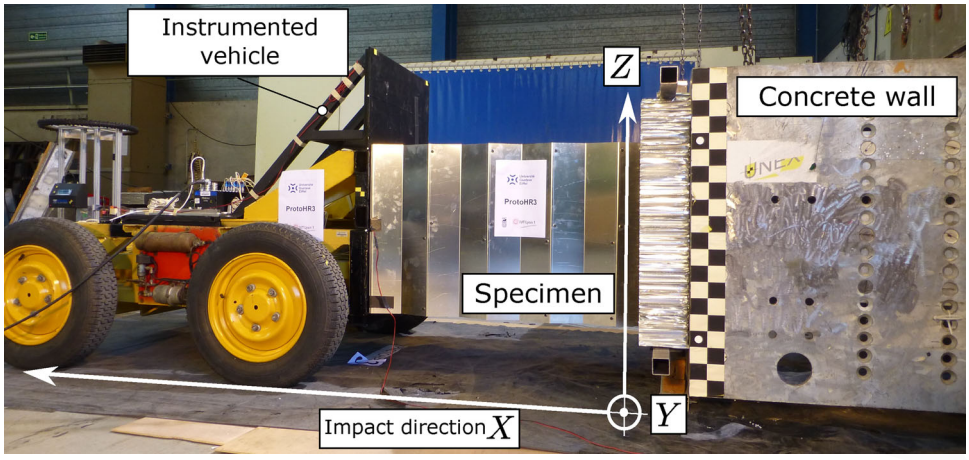

Q4 **Figure 1.** LBMC-crash-track experimental device and the car-crash-cushion specimen.

Table 1. Cameras setup.

Camera	Resolution (pixels)	Shot
1	1024 × 576	(*X*, *Y*) plan
2	768 × 768	(*X*, *Y*) plan
3	1024 × 576	(*X*, *Z*) plan

COLOR Online / B&W in Print

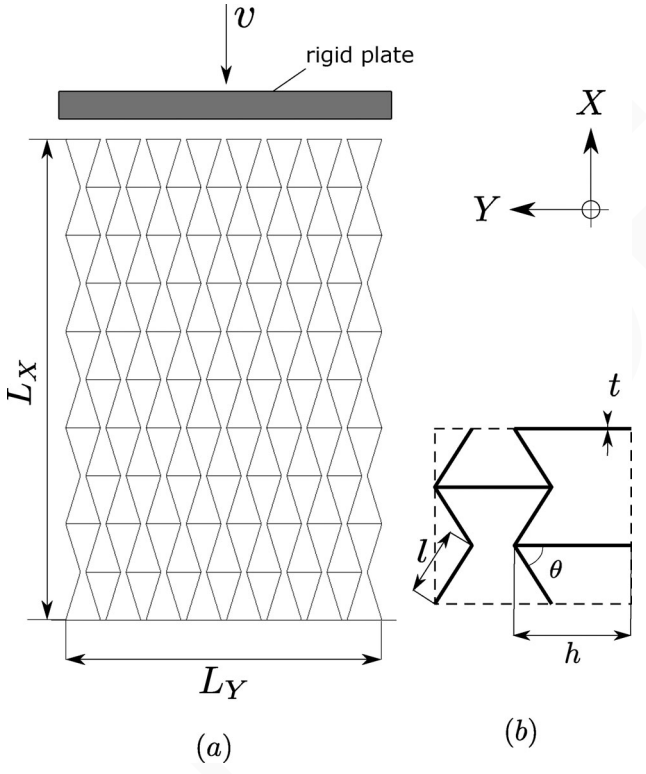

Figure 2. Hexagonal re-entrant honeycomb specimen: (a) whole structure and (b) unit cell detailed with geometric parameters.

Table 2. Geometrical parameters of HR honeycomb specimen.

L_X (*mm*)	L_Y (*mm*)	L_Z (*mm*)	t (*mm*)	l (*mm*)	h (*mm*)	θ (°)
1240	810	690	2	130	90	73

Wavy sheets are bent with a metal press using a V16*mm* vee. The second part is the joint (as shown in Figure 3 and illustrated by the blue line) allowing the assembling of the wavy sheets together. The whole specimen is composed of 16 wavy sheets and 67 joints. Joints and wavy sheets are bolted together with 8 bolts per joint. Each bolt is composed of 1 hexagonal head screw M6x16 ISO4017 class 10.9, 1 hexagonal nut M6 (DIN934) class 10 and 2 plain washers normal type (DIN125-1A) 140HV made of stainless steel. Bolt are tighten at a torque of 11$N.m$. On the front side of the HR honeycomb specimen, 3 metal sheets are riveted to the specimen in order to avoid expansion in the Y direction of the front cells during impact (see Figure 3).

Table 3. Mechanical properties of aluminum AW5754H111.

	E (*MPa*)	$R_{p0.2}$ (*MPa*)	R_m (*MPa*)	$A\%$
AW5754H111	69 000	118	211	26.5

The experimental deformation of the HR honeycomb structure under $v = 13.89m/s$ impact velocity is shown in Figure 5. Before $t = 0.02s$ the Negative Poisson Ratio (NPR) effect is highlighted in the deformation process where the upper layers are crushed. Then, the structure wears down in the Y direction from $t = 0.05s$ to the end of the crash at $t = 0.15s$. The manufacturing process allows to keep the HR honeycomb in one piece all over the impact crashing. The specimen can be considered as a one piece honeycomb without failure or wrenching. These experimental results will then be used to validate the numerical model presented in next Section.

3. Hexagonal re-entrant honeycomb numerical study

3.1. Finite elements analysis

A numerical model of the impacted hexagonal re-entrant honeycomb crash-cushion has been computed, using LS-DYNA explicit solver. In a step of validation, a crashed car of mass $m = 690kg$ is modelled by a rigid plate with an equivalent mass, impacting the HR structure with an initial velocity set to $v = 13.89m/s$, as presented in Figure 2 to match with the measured velocity in the experimental study previously presented in Section 2.

The acceleration γ_x in the X direction on the rigid wall is computed as the ratio of (i) the force (F_X) in the X direction computed in the rigid wall during the crash and (ii) the mass (m) of the wall, as follow:

COLOR Online / B&W in Print

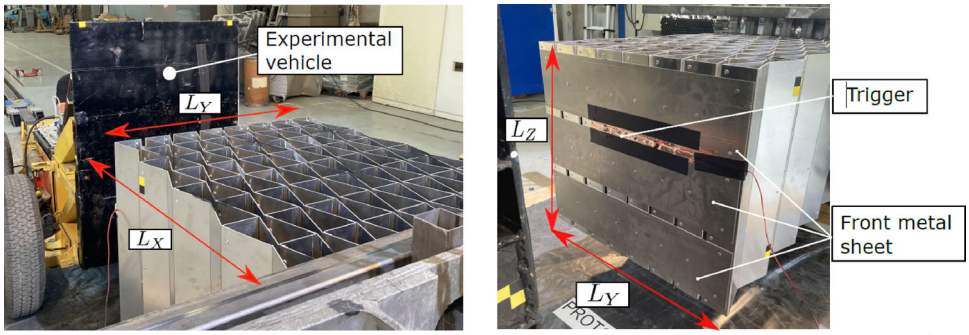

Figure 3. Zoom in on unit HR cell and a joint in the HR honeycomb specimen.

COLOR Online / B&W in Print

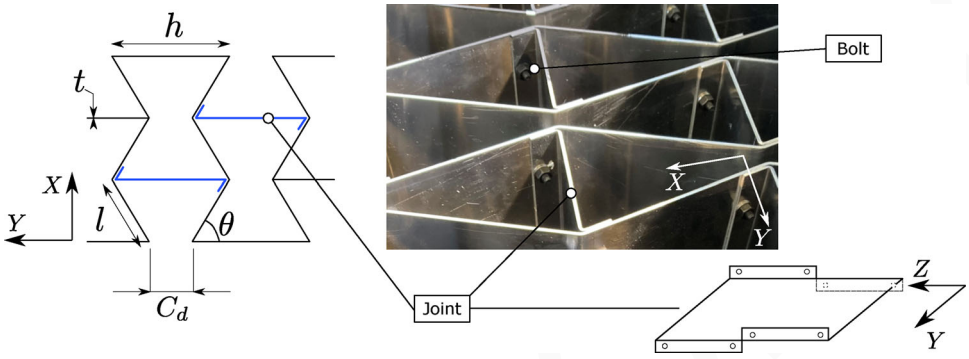

Figure 4. Global view of the HR honeycomb specimen.

COLOR Online / B&W in Print

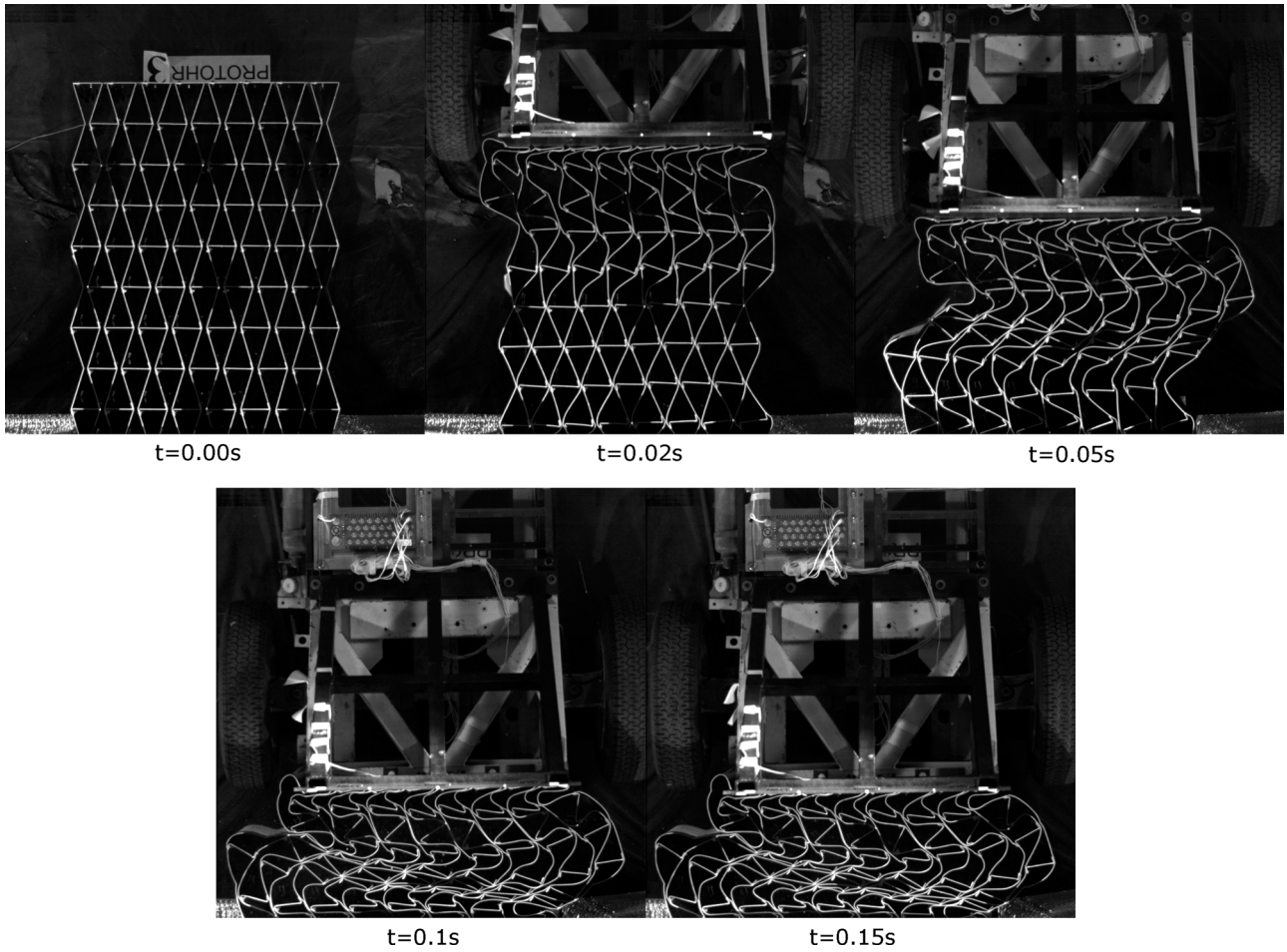

Figure 5. Global deformation of the experimental HR honeycomb specimen over time under crashed condition $v = 13.89m/s$.

$$\gamma_x = \frac{F_X}{m} \quad (1)$$

The acceleration signal is filtered according to European standard (ISO6487 [31]) with a butterworth filter 4 poles at 180 *Hz*. The honeycomb cell walls are meshed using 4-nodes fully-integrated shell elements (Shell 163 in LS-DYNA). Whatever the value of l and h (see Figure 3), the element size is set to $h/4$ to insure a constant number of elements in each cell. An automatic single-self contact (AUTOMATIC_SINGLE_SURFACE) is applied on the whole model by considering a friction coefficient of 0.35. The contact between the rigid plate and the honeycomb structure is considered frictionless. The constitutive material (aluminum alloy) of the cell-wall honeycomb is assumed to be elastic-linear-plastic (MAT_PIECEWISE_LINEAR_PLASTICITY) with Young's modulus E, yield stress σ_{ys}, modulus tangent E_{tan} and constitutive material density ρ given in Table 4, equivalent to the AW 5754 H111 aluminum used for the experimental study presented in Section 2. The mass of the numerical honeycomb structure is equal to the whole structure mass of the experimental specimen, including bolts. As presented before, the failure does not occur during experimental tests, and thus is not considered in the numerical model.

The material of the rigid plate is assumed to be steel and not deformable and thus, neither yield stress nor tangent modulus are needed, as summed up in Table 4.

3.2. Model validation

The experimental and computed results are compared in order to validate the finite elements model presented in Section 3.1. As explained in previous Section 3.1, the numerical rigid wall and experimental vehicle accelerations are compared. Both experimental and numerical signals are filtered using a Butterworth filter with 4 poles at 180 Hz as recommended in the European standard ISO6487 [31].

Firstly, in order to verify the reproducibility of the experimental setup, two experimental crash tests have been conducted on two theoretically identical HR honeycomb specimens called HR1 and HR2. Both experimentations are compared regarding the filtered acceleration signals and the striker displacement over time. The good match between HR1 and HR2 specimen crash tests of the measured accelerations and displacements of the striker are shown in Figures 6 and 7 respectively. These figures express the good reproducibility of the experimental setup. Thus, the mean values of the acceleration and the displacement of the HR1 and HR2 specimens are computed and considered as the experimental data used to validate the numerical model in following sections.

Table 4. Material properties of modelled aluminum alloy and rigid wall steel.

	Material	E (*MPa*)	σ_{ys} (*MPa*)	E_{tan} (*MPa*)	ρ (kg/m^3)
Specimen	Aluminum alloy	69000	118	633	3080
Rigid plate	Not deformable steel	210000	–	–	7800

Figure 8 compares the filtered deceleration computed by the FE model, and measured on the rigid wall (red line) and the measured filtered deceleration of the crashed vehicle (blue line). The mean plateau deceleration $\overline{\gamma_x}$ is computed as the mean deceleration between $t = 0.04s$ and $t = 0.12s$ and values are summed up in Table 5 for both experimental and numerical signals. Furthermore, the maximal deceleration (i.e. the minimal acceleration) is identified as $\min(\gamma_x)$

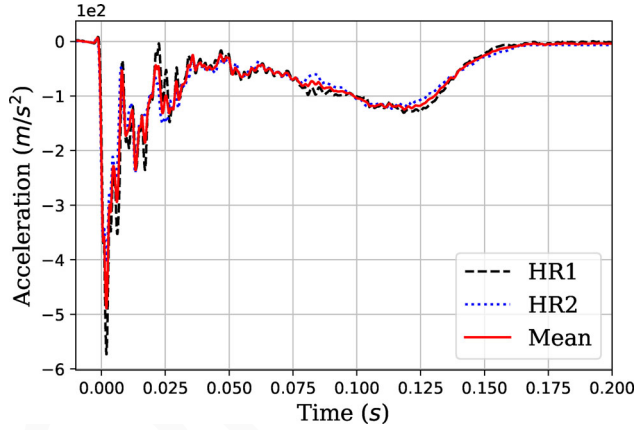

COLOR Online / B&W in Print

Figure 6. Comparison of measured accelerations on the striker under 13.89 *m/s* crash conditions for both specimens and the corresponding mean acceleration.

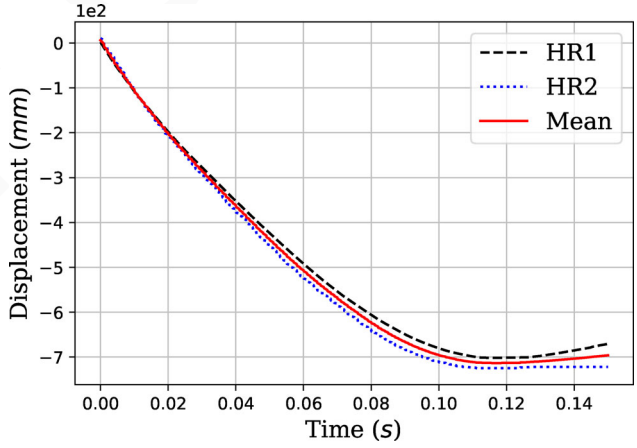

COLOR Online / B&W in Print

Figure 7. Comparison of measured displacement on the striker under 14 m/s crash conditions for both specimens and the corresponding mean displacement.

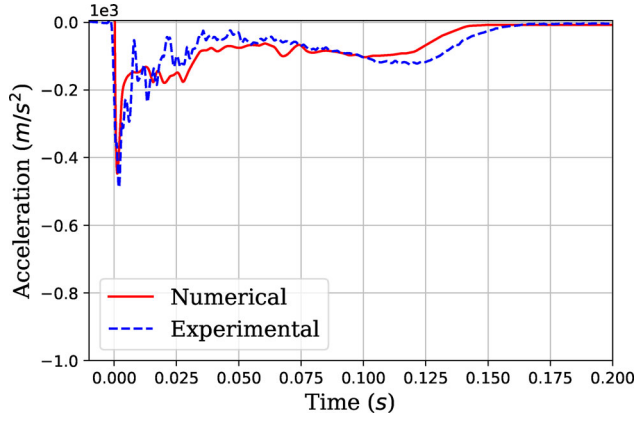

COLOR Online / B&W in Print

Figure 8. Comparison of the acceleration on the striker under 13.89 *m/s* crashed conditions computed by FE analysis and experimentally measured.

Table 5. Comparison of numerical and experimental results.

	$\min(\gamma_x)$ (m/s^2)	$\bar{\gamma}_x$ (m/s^2)	$\max(D_x)$ (mm)
Experimental	−487.89	−78.59	702.2
Numerical	−447.74	−85.13	718.6
r_e (%)	8.41	8.32	2.3

COLOR Online / B&W in Print

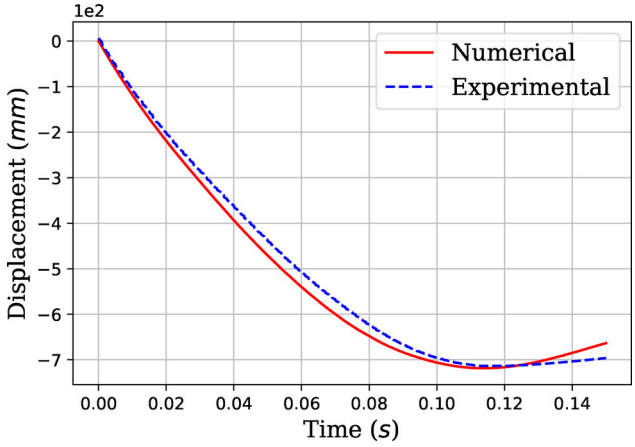

Figure 9. Comparison of the computed and measured striker displacements under 14 m/s crashed conditions.

and occurs at $t = 7.89E{-}5$ seconds on both numerical and experimental acceleration curves.

The displacements of the rigid wall and the crashed vehicle in the X direction are compared in Figure 9. The maximum displacement $\max(D_x)$ is defined as the maximal crushing distance of the striker in the X direction during the impact.

The relative errors $r_{e,\bullet}$ between the experimental and the computed numerical values given in Table 5 are defined as:

$$r_{e,\bullet} = \frac{\bullet_{expe} - \bullet_{simu}}{\bullet_{expe}} \tag{2}$$

where $\bullet_{expe}$ and $\bullet_{simu}$ refer to the considered experimental and numerical values respectively.

The behavior of the whole structure in the FE model is similar to the experimental data given in Section 2. The relative errors around 8% on the acceleration values and less than 3% on the crushing displacement (see Table 5) are acceptable and allow to validate the proposed FE model. The errors can be explained because (i) bolts are not represented in the FE model and (ii) the tested vehicle is not guided during the impact and thus touches the specimen with a tilt angle. The developed and validated FE model will then be used within a parametric optimization process, presented in the next Section.

4. Optimization setup

4.1. Objective function

The force-displacement curve resulting from the numerical model is studied to evaluate the capability of the structure to absorb kinetic energy. One of the crashworthiness criteria is the energy absorption (EA) defined as $EA(x) = \int_0^l F(x)dx$ where l is the total crushing distance, x represents the crushing displacement, and F is the corresponding impact

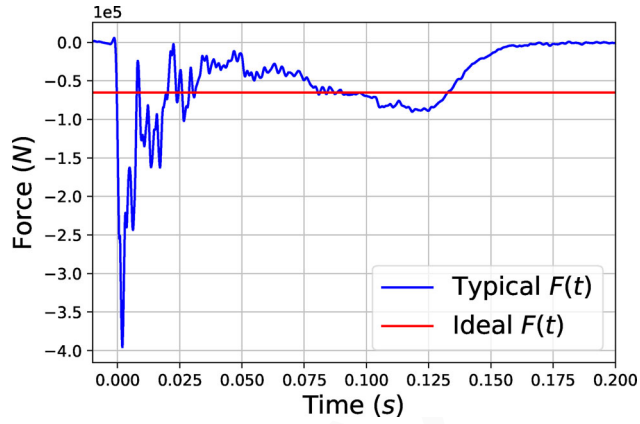

COLOR Online / B&W in Print

Figure 10. Force-time curve for a typical car crash (blue solid line) and the ideal curve (red solid line) for a mass $m = 690kg$.

force as described in Section 3.1. The ideal force-displacement curve to be observed over car crash should be a rectangular function (see Figure 10) [32]. However, focusing only on the force-displacement curve is not safe enough to prevent human being irreversible injuries. Indeed, the European standard is a time-based criterion, due to human tolerances [5]. The European standard uses the Acceleration Index Severity (ASI) to classify the severity of a car crash defined as follows:

$$ASI(t) = \sqrt{\left(\frac{\bar{\gamma}_x}{\hat{\gamma}_x}\right)^2 + \left(\frac{\bar{\gamma}_y}{\hat{\gamma}_y}\right)^2 + \left(\frac{\bar{\gamma}_z}{\hat{\gamma}_z}\right)^2} \tag{3}$$

where $\hat{\gamma}_x$, $\hat{\gamma}_y$ and $\hat{\gamma}_z$ are the thresholds defined in the European standard [5] in the corresponding directions and are equal to $7g$, $5g$ and $6g$ respectively. $\bar{\gamma}_x$, $\bar{\gamma}_y$ and $\bar{\gamma}_z$ are the mean acceleration values of the crashed car over 50 ms in the corresponding directions. For a frontal crash test, the value of ASI has to be lower than 1.4 over a time period of 0.05 s to avoid human irreversible damage. The impact direction being x in this study, the ASI criterion can be written here as:

$$\bar{\gamma}_x < 1.4\hat{\gamma}_x \tag{4}$$

where $\hat{\gamma}_x$ is set to $7g$ [5] with g the gravity acceleration. From Eq. (4), the striker limit force $\bar{F}_L$ can be expressed as:

$$\bar{F}_L = m\bar{\gamma}_x \tag{5}$$

By replacing $\hat{\gamma}_x$ by $7g$ in Eq. (4) it follows:

$$\begin{aligned} \bar{F}_L &< 1.4m\hat{\gamma}_x \\ \bar{F}_L &< 9.8mg \end{aligned} \tag{6}$$

where m is the mass of the striker.

In this way, it is interesting to investigate the force-time curve. The impact force $F(t)$ should attempt to fit a rectangular function where the threshold corresponds to the striker limit force F_L inducing human severe injuries over a period of 0.05 s [5]. Hence, the occupant of the damaged vehicle avoids to suffer a force peak during the crash. Figure 10 illustrates the ideal and typical force-time curves obtained during a car crash.

Commonly in optimization, problems are formulated as follows:

$$\begin{cases} \min f(\alpha_1, \alpha_2, \ldots, \alpha_p) \\ g_i(\alpha_1, \alpha_2, \ldots, \alpha_p) \leq 0 \quad i = 1, 2, \ldots, D \end{cases} \tag{7}$$

where $(\alpha_1, \alpha_2, \ldots, \alpha_p)$ are the p design variables to be optimized, f the objective function defined in a domain called the research domain $\mathcal{D}_f$, g_i the D inequality constraints to be verified.

The newly proposed objective function f is based on the force-time curve measured during the impact. This function measures the difference between the ideal force-time curve and the force-time curve computed in the finite elements model. The objective function is calculated as follows:

$$f(\alpha_1, \alpha_2, \ldots, \alpha_p) = (\bar{F}_L - mean(F_{simu}))^2 \tag{8}$$

where $F_{simu}(\alpha_1, \alpha_2, \ldots, \alpha_p)$ is the value of the computed force over time.

4.2. Input data and design variables

The optimization is performed under an impact velocity v of 14 m/s. The rigid plate striking the top of the structure in the FE model has an initial kinetic energy K_{simu} defined as $K_{car} = \frac{1}{2}mv^2$. From European standard [6] the car mass for light vehicles is set to $m = 900kg$. The studied volume is equal to the volume of actual car cushions located along roads [7,26]. Thus, the volume of the re-entrant honeycomb structure in the FE model is $V_{simu} = L_X \times L_Y \times L_Z$. L_X and L_Y can slightly fluctuate around the defined value to maintain a set of complete cells in the structure. The input data are given in Table 6.

As previously presented in Section 4.1, the computation of the objective function using Eq. (8) depends on the variable set $(\alpha_1, \alpha_2, \ldots, \alpha_p)$. α_p are normalized design variables defined in $[0; 1]$. The normalized mathematical variables used in Eq. (8) correspond to the HR honeycomb geometrical parameters t, l, h and θ respectively (see Table 7).

These variables, presented in Figure 2, are defined in their definition domain $\mathcal{D}_{\beta_p}$ and take into account manufacturing constraints. However, a constraint on variables conducts to a research domain reduction. In the studied case a geometrical constraint must be considered to preserve the hexagonal geometry and is expressed in Eq. (9) according to the geometrical variables previously defined in Figure 2.

$$h - 2l\cos(\theta) > 0 \tag{9}$$

Whatever the variable set, the FE model is automatically generated and performed using LS-DYNA (see Section 3.1) considering all the problem data input.

Table 6. Input data for optimization.

$v(m/s)$	K_{car} (kJ)	$L_X(mm)$	L_Y (mm)	$L_Z(mm)$	$\bar{F}_L$ (N)
14	66.64	800	1200	690	65 373

Table 7. Geometrical correspondence and design domain of all design variables α_p.

Normalized variables α_p	Geometrical variables β_p	$\mathcal{D}_{\beta_p}$
α_1	t	$[0.5; 3.5]$ mm
α_2	l	$[30; 150]$ mm
α_3	h	$[30; 150]$ mm
α_4	θ	$[15; 90[$ $^\circ$

5. Optimization process: Inverse-PageRank-PSO

5.1. Methodology

The optimization method has to be carefully chosen because of the potential non-linearities of the objective function f and the potential interactions between the design variables. The studied problem is intrinsically complex and thus, leads to use a meta-heuristic optimization method. Inverse-PageRank-PSO (I-PR-PSO) is an optimization method particularly adapted to solve non-linear problems [33,34]. This algorithm has shown great global research abilities, that are interesting for solving non-linear problems. The algorithm combines two well known methods by coupling (i) Particle Swarm Optimization (PSO) and (ii) the PageRank (PR) algorithm used by the search engine Google ©.

PSO was first introduced by Kennedy and Eberhart [35], and is inspired by the analysis of bird flock movements. In this method, a population constituted of N_{part} particles, investigates the research domain in order to converge together to the global minimum of the considered objective function. The particles move over the research domain and communicate with each other about their position in the research domain. The communication strategy inside the swarm is called the population topology. Many works have investigated population topologies and suggested improvements such as PSO/ACO, PSO-SQP, PSO-GWO or I-PR-PSO [33,36–38].

In I-PR-PSO, the particles connectivity can be seen as an oriented graph. In this way, the influence of the particles on the others is weighed regarding their respective fitness values. A particle which exhibits a low value of fitness influences more the next position of other particles than a particle exhibiting a high value of fitness (for a minimization problem). The position $\mathbf{X}_i^{k+1}$ of the particle i at the iteration $k+1$ is calculated as follows:

$$\begin{cases} \mathbf{V}_i^{k+1} = \omega \times \mathbf{V}_i^k + c_1 \times rand_1 \times (\mathbf{P}_{i,best}^{k+1} - \mathbf{X}_i^k) + c_2 \times rand_2 \times \sum_{j=1}^{n} \mathbf{C}_{ij} \times (\mathbf{P}_{j,best}^{k+1} - \mathbf{X}_i^k) \\ \mathbf{X}_i^{k+1} = \mathbf{X}_i^k + \mathbf{V}_i^{k+1} \end{cases} \tag{10}$$

where $\mathbf{P}_{i,best}$ is the best personal position of the particle i, $\mathbf{V}_i^k$ is the velocity[1] of particle i at iteration k, ω is the inertia weight of the particle, $rand_1$ and $rand_2$ are random numbers in $[0;1]$, c_1 and c_2 are coefficients representing the social and individual behavior of the particle and $\mathbf{C}$ is the stochastic connectivity matrix defined by the Inverse-PageRank algorithm. Particle i is influenced by all the particles of the swarm, and their respective influences are given by the components of the jth line of $\mathbf{C}$. The component $\mathbf{C}_{ij}$ corresponds to the influence of all particles on particle i. Indeed, the particle swarm can be seen as a Markov chain, in which each link represents the influence of a particle on an other one. In the same way as in the search engine Google, a PageRank score is attributed to each particle according to its own success, that allows to build the stochastic connectivity matrix $\mathbf{C}$. The reader can refer to [34] for more details about I-PR-PSO.

I-PR-PSO is applied to the FE model of the HR honeycomb crashing (see Section 3.1) in order to find the best combination of the geometrical parameters to efficiently absorb the kinetic energy in car-crashed conditions. In other words, the algorithm is employed to find a parameter set for which the objective function f defined in Section 4.1 reaches a minimum. In the considered problem, each particle i is represented by a vector $\mathbf{X}_i^k$ containing the position of the particle in the research domain $\mathcal{D}_f$, at iteration k. The particle coordinates correspond to normalized values of the design variables in their respective domains as follows:

$$\mathbf{X}_i^k = \begin{pmatrix} \alpha_{1,i}^k \\ \alpha_{2,i}^k \\ \alpha_{3,i}^k \\ \alpha_{4,i}^k \end{pmatrix} \tag{11}$$

For each particle i, at each iteration k, a FE calculation is launched, and the value of the objective function $f(\mathbf{X}_i^k)$ is calculated by using Eq. (8).

As explained in Section 4.2, the problem is highly constrained because of the optimization constraint imposing $h-2l\cos(\theta)>0$. A simple penalty method is applied to a particle that does not respect the condition [39]. In the studied case, if Eq. 9 is not verified, the fitness value is not computed in order to save computational time and because the structure might be unmanufacturable. A penalty value, set to $10E30$, is attributed to the considered particle to isolate it from the swarm. Thus, the particle which does not verify Eq. (9) has an insignificant influence on its pairs.

5.2. I-Pr-PSO parameters

As explained in the latter Section, I-PR-PSO parameters have to be carefully chosen to ensure the algorithm convergence. As for classical PSO, a large diversity of parameter sets are discussed [40–45]. Indeed, the parameter set is strongly problem-dependent as demonstrated in [46].

The values of I-PR-PSO parameters (ω, c_1 and c_2) are summed up in Table 8. The algorithm can be considered as converged either when the number of iterations k reaches the maximum number of iterations (set by the user) $it_{PSO,MAX}$ or when the value of the best position does not improve after it_{conv} iterations.

Parameters can be considered as a good selection when the algorithm presents an efficient convergence curve (i.e. the evolution of the best fitness value found over iterations). So, in the following optimization process, a convergence study is presented, where I-PR-PSO parameters have been empirically found.

The values of c_1 and c_2 gradually decrease while I-PR-PSO process progresses. Δc is subtracted to c_1 and c_2, at each iteration k.

Table 8. I-PR-PSO parameters used in Eq. (10).

ω	$c1$	$c2$	Δ_c	N_{part}	$it_{PSO,MAX}$	it_{conv}
0.6	1.5	1.5	0.033	8	45	30

5.3. Obtained results

5.3.1. Optimal structure

This section presents the results obtained by the optimization process. The numerical model used within the optimization has been previously presented in Section 3.1, and validated based on experimental tests presented in Section 3.2. Four design variables have been optimized, corresponding to the geometrical parameters of the HR honeycomb structure. The optimization algorithm, Inverse-PageRank-PSO, proposes optimized values of these parameters, effectively minimizing the objective function defined in Section 4.1. The convergence curve, presenting the best values of the objective function found so far during the optimization process and the corresponding cell dimensions, is plotted in Figure 11. Moreover, the tested values of the design variables, which are the positions of the particles during the process, are scattered in Figure 12. As one can see in these figures: (i) the research domain is explored until the 20^{th} iteration, where the swarm switches from exploration to exploitation, the particles converging together, by following each other, to promising zones of the research domain. (ii) The objective function is optimized, switching from an

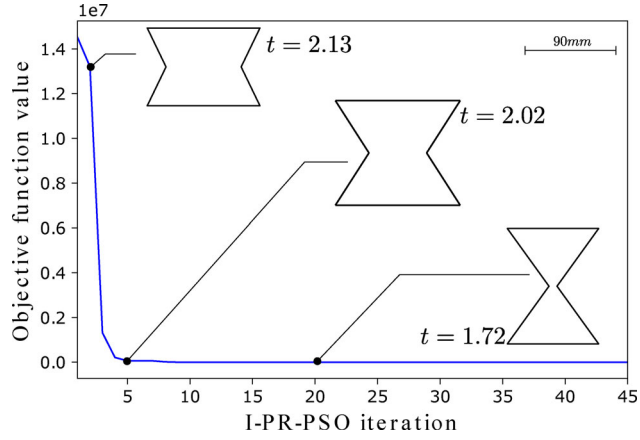

COLOR Online / B&W in Print

Figure 11. Convergence curve of the objective function for HR honeycomb optimization and corresponding cell dimensions.

COLOR Online / B&W in Print

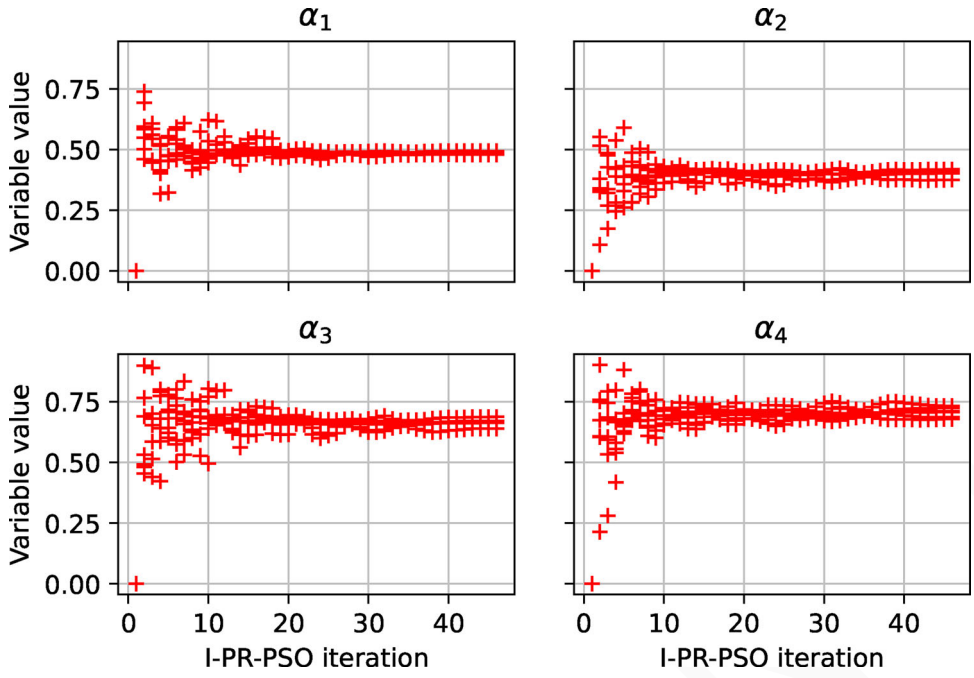

Figure 12. Evolution of particles position in the research domain for HR honeycomb optimization.

Table 9. HR honeycomb optimal geometrical parameters for energy absorption.

t(mm)	l(mm)	h(mm)	$\theta(^\circ)$
1.95	77.90	109.27	60.705

initial value of $G_{best} = 1.45E + 07$, to a minimal value of $G_{best} = 68.94$ at the end of the optimization process.

The optimal values of the design variables are given in Table 9, corresponding to the best values of the geometrical parameters of the HR honeycomb.

A FE analysis is carried out on the optimal structure. The evolution of the force computed on the striker over time $F_{opt}(t)$ is presented in Figure 13. As one can see, due to the fitting process induced by the using of the objective function presented in Section 4.1, the force actually fits the limit force $\bar{F}_L$, and remains at this plateau value during the whole crash. Therefore, the optimization process, by minimizing the objective function, permits to smooth the force suffered by the vehicle occupant, limiting the human damage. The plateau force obtained in Figure 13 induces a quasi-linear decreasing of the striker kinetic energy, with a slope of $6.46E + 08$, as presented in Figure 14. As one can see, at the crushing beginning, the kinetic energy slope is steeper $(1.17E + 11)$, due to the force $F_{opt}(t)$ exhibiting a peak at the crushing instant. However, the acceleration criterion, previously defined in Eq. (3) and being proportional to $F_{opt}(t)$, is equal to $9.79g$, which is inferior to the limit of $9.8g$ imposed by European standards [5]. The optimal HR honeycomb behavior is then smoothly absorbing kinetic energy as a cushion device. The optimal HR honeycomb structure absorbs 79% of the initial energy. The optimization of the mean force over time, as presented in Eq. (8), allows the kinetic energy absorption to be spread over a sufficiently long time to minimize the damage to the vehicle occupants, as well as verifying the European standard

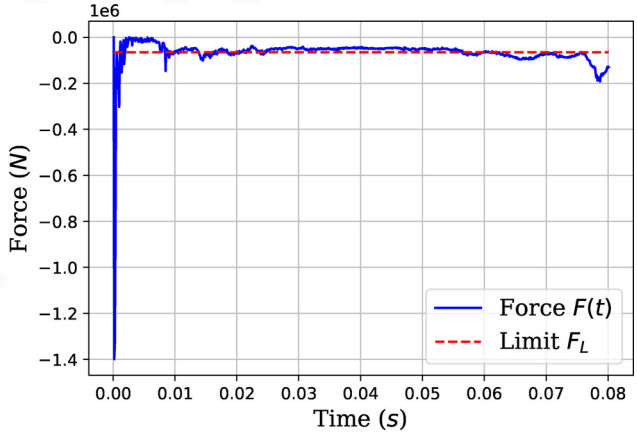

COLOR Online / B&W in Print

Figure 13. Force curve $F(t)$ and limit force $\bar{F}_L$ of the optimal HR honeycomb.

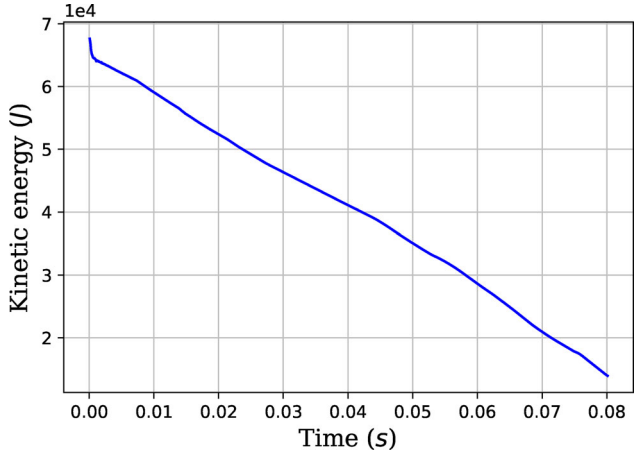

COLOR Online / B&W in Print

Figure 14. Kinetic energy absorption over the time for optimal HR honeycomb.

criterion. As one can see in Figure 15 presenting the structure deformation over time, the negative Poisson ratio effect occurs. At t = 0.018s, a V-mode deformation is observed on

COLOR Online / B&W in Print

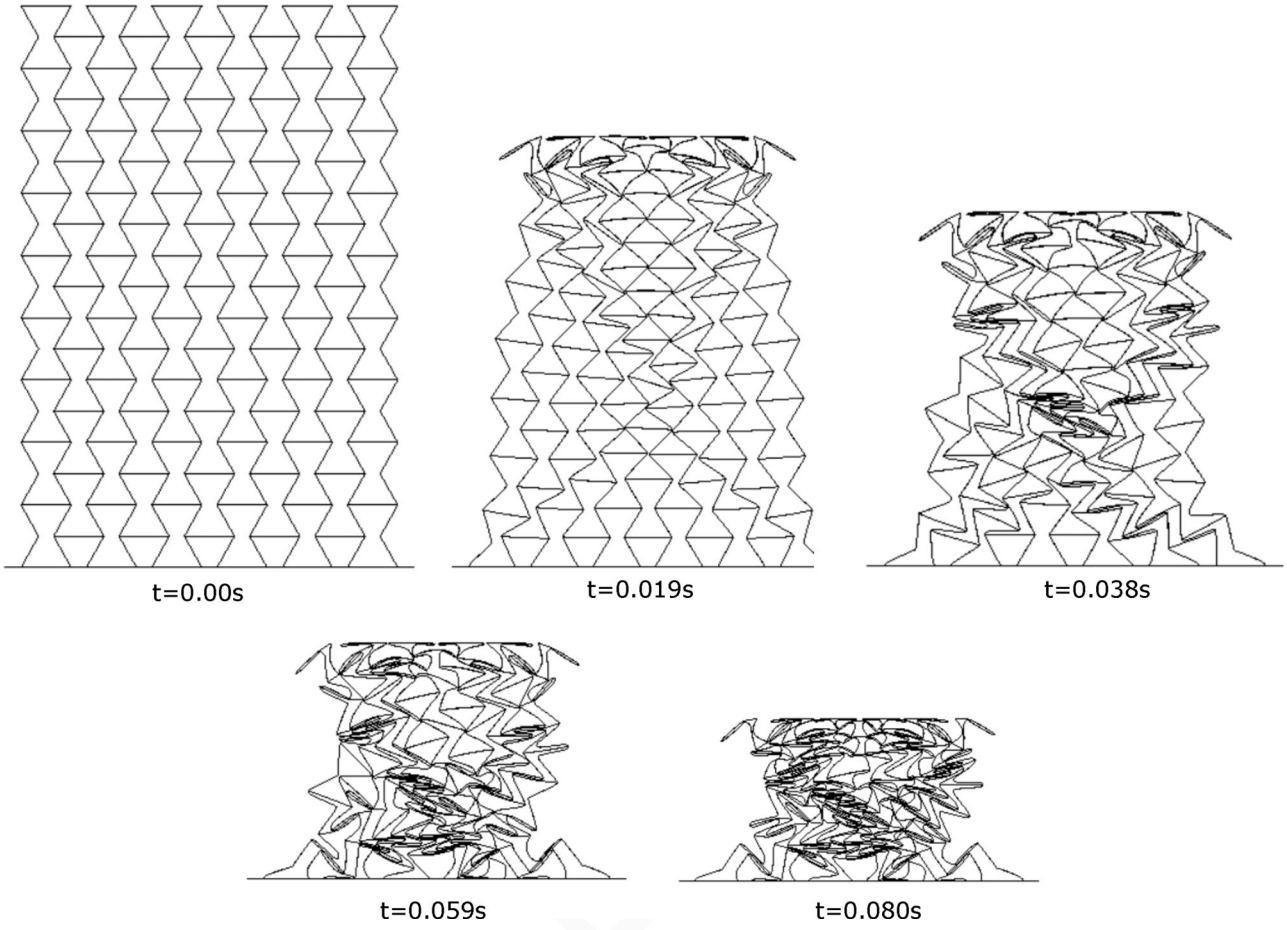

Figure 15. Finite elements simulation performed on the optimal HR honeycomb structure.

the top of the structure, while a double horizontal V-mode deformation occurs at t = 0.06s. This behavior induces the efficient kinetic energy absorption, as it was demonstrated in [47]

5.3.2. Off-centered and titled crash test on the optimal structure

The optimal structure presents a good efficiency under frontal impact conditions as presented in Section 5.3.1. In road safety area, the probability to crash a car-cushion device in a perfectly frontal impact condition is very low and thus, the behavior of the HR honeycomb structure under off-centered and titled impact conditions must be verified. In this Section, two impact configurations described in the European Standard EN1317-3 [6] are considered on the optimal HR honeycomb structure obtained in the previous Section 5.3.1. The impact configurations can be described with two parameters, the titled angle and the off-set distance applied to the rigid wall in the FE model defined in Section 3.1. The off-set distance is defined as $\frac{1}{4} \times L_Y$ in EN1317-3 leading to the impact parameters given in Table 10. The trajectories of the center of gravity of the rigid wall in the three configurations are described in Figure 16.

Two new FE computations are added to the FE analysis carried out on the optimal HR honeycomb structure (Section 5.3.1) in the N °1 and N °2 impact configurations given in Table 10. Energy absorption curves and force curves are presented and compared in Figures 17 and 18 respectively. These figures demonstrate that the global behavior of the optimal HR honeycomb is not sensitive to the impact conditions. Indeed, whatever the impact configuration considered, the kinetic energy absorbed after 0.08 s is in a range of 70 to 79% of the initial kinetic energy. Moreover, the energy absorption curves remain quasi-linear for all impact configurations. For both frontal impacts, the curves are similar in the first 0.03 s of the crash, with a steeper slope at the beginning. The tilted impact presents no steeper slope at the beginning, and thus is much smoother than the two other impact conditions. The soft decreasing of energy absorption is also noticeable on the not-filtered force-time curve given in Figure 18. The part of kinetic energy absorbed by the HR honeycomb structure after t = 0.08s are given in Table 11 for the three configurations. The tilted-force is a quasi-linear plateau. The centered and off-centered force curves present a plateau that reflects the quasi-linear behavior of the energy absorption curve while there is a peak force at the beginning of the contact. The plateau force under tilted configuration is lower than the

Table 10. Impact configuration.

Configuration	Titled angle (°)	Off-set (*mm*)
N °0	0	0
N °1	0	205
N °2	15	0

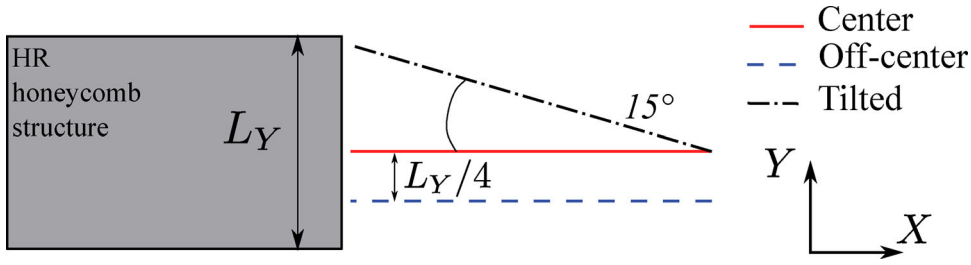

Figure 16. Center of gravity trajectories of the three impact configurations.

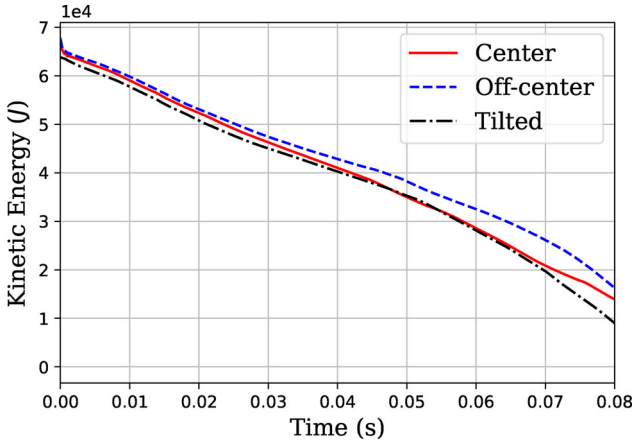

Figure 17. Energy absorption curves computed on the optimal HR honeycomb structure under i) frontal ii) off-centered frontal and iii) tilted impact configurations.

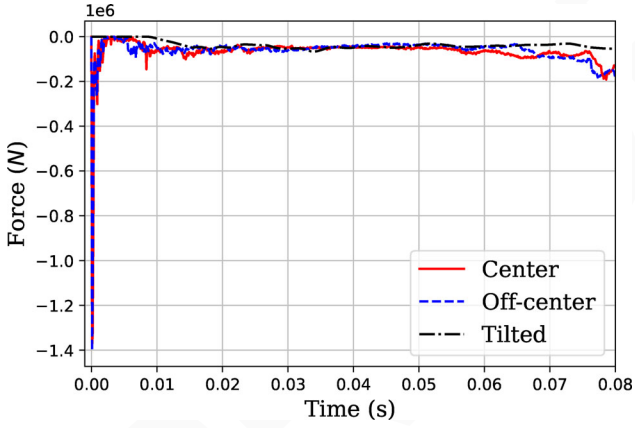

Figure 18. Force-time curves computed on the optimal HR honeycomb structure under i) frontal ii) off-centered frontal and iii) tilted impact configurations.

Table 11. Results on the optimal HR structure under different impact configurations.

Configuration	Kinetic energy absorbed (%)	ASI
N °0	79.0	1.311
N °1	75.9	1.232
N °2	70.5	0.804

frontal off-centered and the centered configurations. Indeed, the frontal centered configuration is the most critical human being configuration and thus presents a higher value of the plateau force. To illustrate these curves, the ASI (defined in Section 4.1) are computed for the three configurations and given in Table 11. For all the configurations, the ASI value is lower than the limit set to 1.4 by the European standard [5].

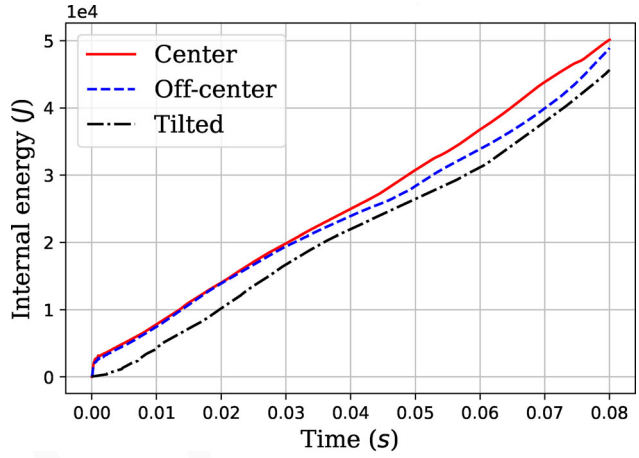

Figure 19. Finite elements simulation performed on the optimal HR honeycomb structure in the tilted impact configuration.

The numerical deformation of the optimal HR honeycomb under off-centered and tilted impact configurations are illustrated in Figures 19 and 20 respectively. Around $t = 0.02s$, the negative Poisson ratio effect allows a densification of the structure at the centre of the honeycomb while the upper part of the structure is also crushed. The quasi-linear energy decreasing described in Section 5.3.1 is allowed thanks to the deformation occurring in the whole structure at the same time. Indeed, the optimization process carried out on the FE model has led to the design of a structure able to absorb energy mostly by plastic deformation spread on the whole structure at the same time. Around 74% of the initial kinetic energy is absorbed by plastic deformation as illustrated in Figure 21 in which the internal energy in the HR honeycomb over time is plotted for the three different impact configurations.

Whatever the impact conditions, the optimal HR honeycomb structure obtained in this optimization study is efficient in car crash energy absorption, and meets the European standard criterion defined in Section 4.1.

6. Discussion and conclusion

The hexagonal re-entrant honeycomb is a promising structure in energy absorption partly because of its auxetic behavior. This study investigates an optimal geometry of HR honeycomb structure under car-crashed impact velocity which corresponds to speed limitations in the European standard [5].

An experimental study is conducted on a HR honeycomb specimen which is impacted by a rigid vehicle launched at $v = 14m/s$. The specimen, made of aluminum and

COLOR Online / B&W in Print

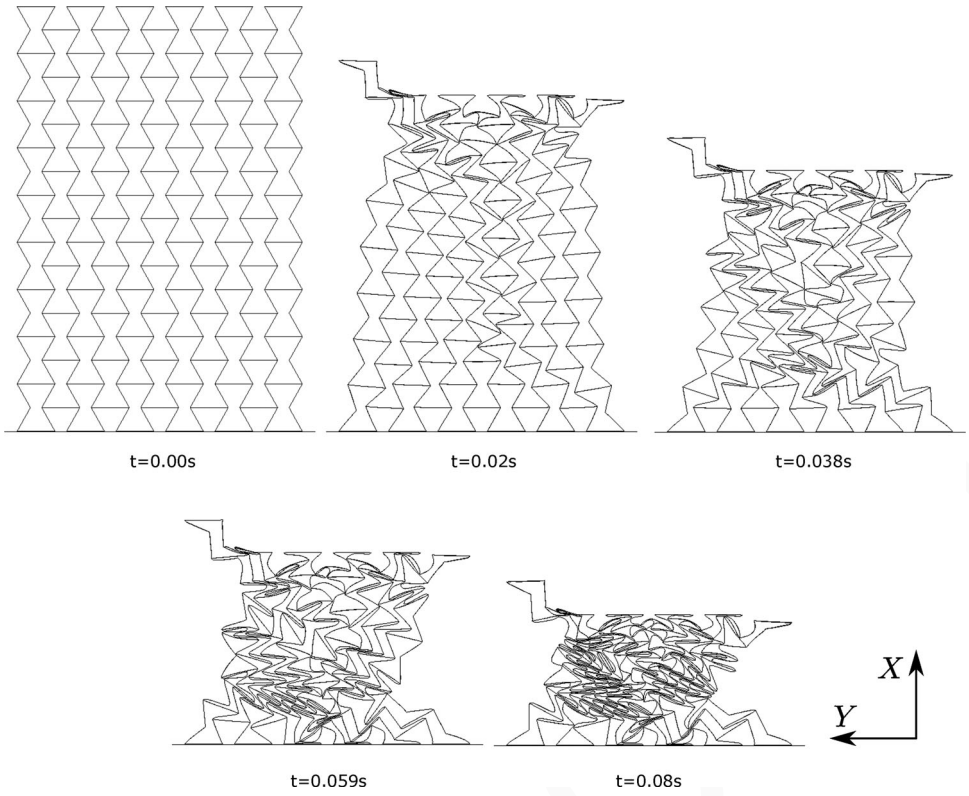

Figure 20. Internal energy curves computed on the optimal HR honeycomb structure under i) frontal ii) off-centered frontal and iii) tilted impact configurations.

COLOR Online / B&W in Print

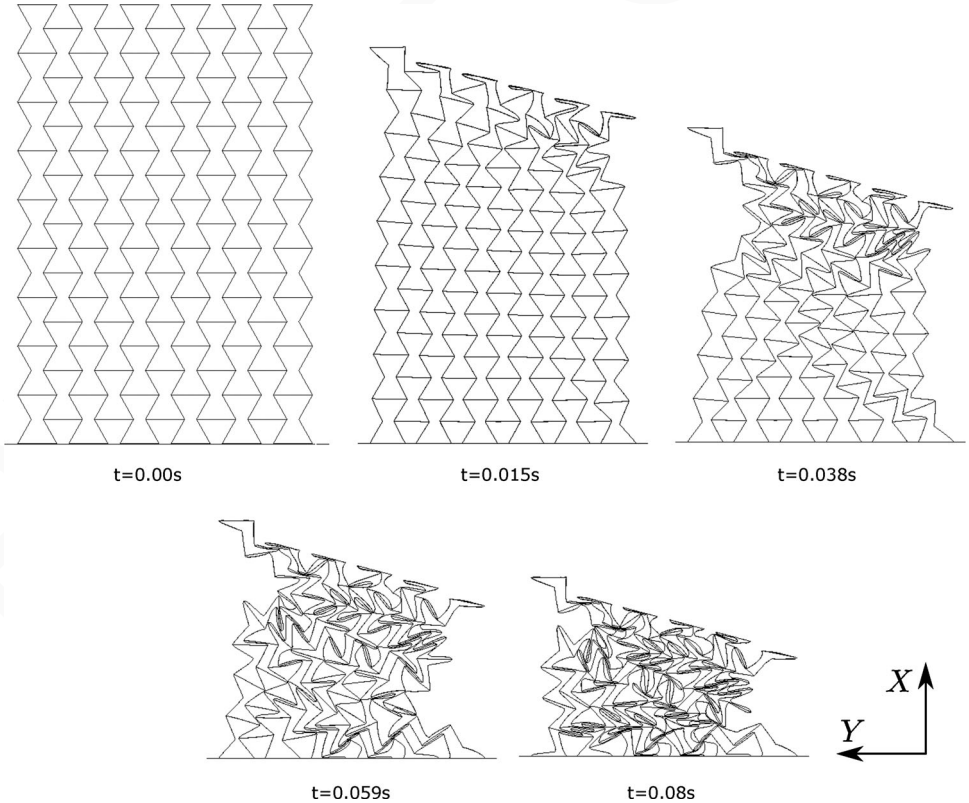

Figure 21. Finite elements simulation performed on the optimal HR honeycomb structure in the off-centered impact configuration.

conventionally assembled, is on the scale of car-cushion devices. The experimental analysis led to the FE model validation by comparing measured and computed signals of displacement and acceleration. The relative differences around 8% are considered as acceptable and can be due to assembly simplifications in the FEM.

The objective function proposed shows a good efficiency to measure the absorbing capabilities of the considered

structure to be optimized. This new objective function is based on the European standard criteria [6], and conducts to optimize the force-time curve, by trying to fit an ideal rectangular force-time curve. This objective function is computed with the validated FE model, and depends on the HR honeycomb geometry. Four parameters, t, l, h and θ are defined to describe the honeycomb structure. Moreover, a geometrical constraint is modeled and corresponds to manufacturing considerations.

A global optimization process is applied to the HR honeycomb structure and performed with the Inverse-PageRank-PSO (I-PR-PSO) algorithm. This meta-heuristic method has shown high efficiency in complex real-problem optimization. A penalty method is applied to I-PR-PSO in order to apprehend the geometrical constraint of the HR honeycomb structure. The optimal structure found presents a quasi-linear energy absorption curve, that can be considered as ideal, with 80% of the initial kinetic energy absorbed. This performance will be increased in real-world application because the crashed car also absorbs energy due to its own deformation not considered in this study. Finally, the optimal HR honeycomb structure obtained in the optimization process is tested under three different impact configurations as defined in the European standard EN1317-3. The optimal HR structure presents high performance in energy absorption whatever the impact configuration considered. This study gives an optimization process with a validated objective function to design new car crash cushion devices, and could be used in other crash contexts such as different materials and impact velocities, or to design truck-cushion devices by adjusting the mass of the striker.

Note

1. Called" velocity" in the literature, V is actually a displacement imposed to particles.

Disclosure statement

Q2 No potential conflict of interest was reported by the authors.

Funding

The authors acknowledge the 'Délégation à la Sécurité Routière' (Road safety Delegation) of French government for their financial support (Convention 21 02 59 88 39).

References

[1] Papka SD, Kyriakides S. In-plane compressive response and crushing of honeycomb. J Mech Phys Solids. 1994;42(10):1499–1532.
[2] Gibson LJ. Cellular solids. MRS Bull. 2003;28(4):270–274.
[3] Ruan D, Lu G, Wang B, et al. In-plane dynamic crushing of honeycombs—a finite element study. Int J Impact Eng. 2003;28(2):161–182.
[4] Scarpa F, Panayiotou P, Tomlinson G. Numerical and experimental uniaxial loading on in-plane auxetic honeycombs. J Strain Anal Eng Des. 2000;35(5):383–388.
[5] European Standard. EN1317-1. road restraint systems, part 1: Terminology and general criteria for test methods; 2010.
[6] European Standard. EN1317-3. road restraint systems - part 3: Performance classes, impact test acceptance criteria and test methods for crash cushions; 2010.
[7] Crash Cushion. Road barrier - SMA 50P. https://www.smaroad-safety.com/en/gamma/view/8/50p.
[8] Hou X, Deng Z, Zhang K. Dynamic crushing strength analysis of auxetic honeycombs. Acta Mech Solida Sin. 2016;29(5):490–501.
[9] Hu L, Zhou MZ, Deng H. Dynamic crushing response of auxetic honeycombs under large deformation: theoretical analysis and numerical simulation. Thin-Walled Struct. 2018;131:373–384.
[10] Imbalzano G, Linforth S, Ngo TD, et al. Blast resistance of auxetic and honeycomb sandwich panels: comparisons and parametric designs. Compos Struct. 2018;183:242–261.
[11] Dirrenberger J, Forest S, Jeulin D. Elastoplasticity of auxetic materials. Comput Mater Sci. 2012;64:57–61.
[12] Sanami M, Ravirala N, Alderson K, et al. Auxetic materials for sports applications. Proc Eng. 2014;72:453–458.
[13] Alderson A, Alderson K. Auxetic materials, proceedings of the institution of mechanical engineers. Part G: J Aerospace Eng. 2007;221(4):565–575.
[14] Lakes R. Foam structures with a negative poisson's ratio. Science. 1987;235(4792):1038–1040.
[15] Evans KE. Auxetic polymers: a new range of materials. Endeavour. 1991;15(4):170–174.
[16] Evans KE, Alderson A. Auxetic materials: functional materials and structures from lateral thinking. Adv Mater. 2000;12(9):617–628.
[17] Dirrenberger J, Forest S, Jeulin D, et al. Homogenization of periodic auxetic materials. Proc Eng. 2011;10(0):1847–1852.
[18] Masson R, Bornert M, Suquet P, et al. An affine formulation for the prediction of the effective properties of nonlinear composites and polycrystals. J Mech Phys Solids. 2000;48(6–7):1203–1227.
[19] Dong Z, Li Y, Zhao T, et al. Experimental and numerical studies on the compressive mechanical properties of the metallic auxetic reentrant honeycomb. Mater Des. 2019;182:108036.
[20] Javadi AA, Faramarzi A, Farmani R. Design and optimization of microstructure of auxetic materials. Eng Comput. 2012;29(3):260–276.
[21] Pal A, Bertoldi K, Pham MQ, et al. Optimal turbine blade design enabled by auxetic honeycomb. Smart Mater Struct. 2020;29(12):125004.
[22] Duncan O, Shepherd T, Moroney C, et al. Review of auxetic materials for sports applications: Expanding options in comfort and protection. Appl Sci. 2018;8(6):941.
[23] Masters I, Evans K. Models for the elastic deformation of honeycombs. Compos Struct. 1996;35(4):403–422.
[24] Wang T, Li Z, Wang L, et al. Crashworthiness analysis and collaborative optimization design for a novel crash-box with re-entrant auxetic core. Struct Multidisc Optim. 2020;62(4):2167–2179.
[25] Qi C, Pei L-Z, Remennikov A, et al. Parametric study and optimization of the protect system containing a re-entrant hexagon cored sandwich panel under blast impact. Compos Struct. 2020;252:112711.
[26] Crash Cushion. Road Barrier - SMA 110W. https://www.smaroadsafety.com/en/gamma/view/14/110w.
[27] Qiu N, Gao Y, Fang J, et al. Topological design of multi-cell hexagonal tubes under axial and lateral loading cases using a modified particle swarm algorithm. Appl Math Modell. 2018;53:567–583.
[28] Xiang J, Du J. Energy absorption characteristics of bio-inspired honeycomb structure under axial impact loading. Mater Sci Eng: A. 2017;696:283–289.

[29] Gao Q, Zhao X, Wang C, et al. Multi-objective crashworthiness optimization for an auxetic cylindrical structure under axial impact loading. Mater Des. 2018;143:120–130.
[30] ExpéChoc. LBMC experimental plateform in crash. https://lbmc.univ-gustave-eiffel.fr/plateformes/expechoc-plateforme-dexperimentation-en-choc.
[31] European Standard, ISO 6487. Road vehicles — measurement techniques in impact tests — instrumentation; 2015.
[32] Clough EC, Plaisted TA, Eckel ZC, et al. Elastomeric microlattice impact attenuators. Matter. 2019;1(6):1519–1531.
[33] Di Cesare N, Chamoret D, Domaszewski M. A new hybrid pso algorithm based on a stochastic markov chain model. Adv Eng Software. 2015;90:127–137.
[34] Di Cesare N, Domaszewski M. A new hybrid topology optimization method based on i-pr-pso and eso. application to continuum structural mechanics. Comput Struct. 2019;212:311–326.
[35] Kennedy J, Eberhart R. Particle swarm optimization. In: Proceedings of ICNN'95-International Conference on Neural Networks. Vol. 4. IEEE; 1995. p. 1942–1948.
[36] Holden N, Freitas AA. A hybrid pso/aco algorithm for discovering classification rules in data mining. J Artif Evol Appl. 2008;2008:1–11.
[37] Victoire TAA, Jeyakumar AE. Hybrid PSO–SQP for economic dispatch with valve-point effect. Electr Power Syst Res. 2004;71(1):51–59.
[38] Şenel FA, Gökçe F, Yüksel AS, et al. A novel hybrid pso–gwo algorithm for optimization problems. Eng Comput. 2019;35(4):1359–1373.
[39] Parsopoulos KE, Vrahatis MN. Particle swarm optimization method for constrained optimization problems. In: Intelligent technologies–theory and application: new trends in intelligent technologies. Vol. 76; 2002. p. 214–220.
[40] Ozcan E, Mohan CK. Particle swarm optimization: surfing the waves. In: Proceedings of the 1999 Congress on Evolutionary Computation-CEC99 (Cat. No. 99TH8406). Vol. 3; 1999. p. 1939–1944.
[41] Clerc M. The swarm and the queen: towards a deterministic and adaptive particle swarm optimization. In: Proceedings of the 1999 congress on evolutionary computation-CEC99 (Cat. No. 99TH8406). Vol. 3; 1999. p. 1951–1957.
[42] Clerc M, Kennedy J. The particle swarm-explosion, stability, and convergence in a multidimensional complex space. IEEE Trans Evol Comput. 2002;6(1):58–73.
[43] Trelea IC. The particle swarm optimization algorithm: convergence analysis and parameter selection. Inf Process Lett. 2003;85(6):317–325.
[44] Armaghani DJ, Hajihassani M, Mohamad ET, et al. Blasting-induced flyrock and ground vibration prediction through an expert artificial neural network based on particle swarm optimization. Arab J Geosci. 2014;7(12):5383–5396.
[45] Hajihassani M, Armaghani DJ, Monjezi M, et al. Blast-induced air and ground vibration prediction: a particle swarm optimization-based artificial neural network approach. Environ Earth Sci. 2015;74(4):2799–2817.
[46] Suganthan PN. Particle swarm optimiser with neighbourhood operator. In: Proceedings of the 1999 Congress on Evolutionary Computation-CEC99 (Cat. No. 99TH8406). Vol. 3; 1999. p. 1958–1962.
[47] Jiang H, Ren Y, Jin Q, et al. Crashworthiness of novel concentric auxetic reentrant honeycomb with negative poisson's ratio biologically inspired by coconut palm. Thin-Walled Struct. 2020;154:106911.

Q3